Surface roughness dating of long-runout landslides near Oso, Washington (USA), reveals persistent postglacial hillslope instability

Sean R. LaHusen[1], Alison R. Duvall[1], Adam M. Booth[2], and David R. Montgomery[1]
[1]Department of Earth and Space Sciences, University of Washington, Box 351310, Seattle, Washington 98195, USA
[2]Department of Geology, Portland State University, 1721 SW Broadway, Portland, Oregon, 97201 USA

ABSTRACT

Establishing regional landslide chronologies is necessary to advance from hazard recognition to risk assessment, and to understand the evolution of landslide-prone terrain. Despite recent advances in landslide mapping due to the availability of high-resolution lidar imagery, estimating the timing of slope failures remains a challenge. Here we present a new integrated approach to dating landslides on a regional scale by augmenting quantitative surface roughness analysis with radiocarbon dating and numerical landscape modeling. We calibrate a roughness-age curve, which we use to date 25 deep-seated landslides in glacial sediment surrounding the catastrophic A.D. 2014 Oso landslide along the North Fork Stillaguamish River in Washington State (USA). Lidar bare-earth images show a high density of long-runout landslides in this region. Using our roughness-age curve, we estimate an average Holocene landslide frequency of 1 every 140–500 yr, and show that the 2014 Oso landslide was the latest event in an active history of slope failures throughout the Holocene. With each landslide, substantial sediment is delivered to the North Fork Stillaguamish River, driving shifts in the active channel that ultimately affect the pattern of landslides across the valley. The high frequency of landslides in this area, where river incision and isostatic uplift rates have dropped dramatically since peaking soon after ice retreated from the region, shows that landscapes inundated by glacial sediment do not require dramatic changes in base level to remain highly unstable for tens of thousands of years.

INTRODUCTION

Our ability to perform rapid and precise geomorphometric analyses of landslides has increased dramatically in the past decade with new availability of high-resolution lidar elevation data (Roering et al., 2013). Despite much-needed progress in remote landslide mapping, the challenges of dating landslides still limit our understanding of the causes of these mass movements, and hamper our ability to implement full statistical assessments of landslide hazard (Lang et al., 1999; Pánek, 2015). Hazard assessments require knowledge of landslide probability within a given period of time (Morgan et al., 1992; Bell and Glade, 2004; Sterlacchini et al., 2007), yet finding the appropriate dateable material across large areas can be difficult and cost prohibitive.

In this study we use radiocarbon dates to calibrate a surface roughness-age function that predicts how the surface roughness of landslide deposits decreases over time. We apply this new approach to the area surrounding the devastating A.D. 2014 Oso landslide, along the North Fork Stillaguamish River valley in western Washington State (USA) (Fig. 1). Much of the destruction caused by the Oso landslide was due to its mobility, quantified by a low height to runout-length ratio (H:L) of 0.10 (Keaton et al., 2014; Iverson et al., 2015). Lidar bare-earth imagery reveals numerous deep-seated landslides of similar morphology surrounding the Oso failure site. Crosscutting relationships indicate that these landslides occurred over multiple generations (Haugerud, 2014), yet their absolute ages remain undetermined. Our analysis places new absolute ages on two large landslides and allows us to estimate the timing of failure for other landslides across the study area.

BACKGROUND

When the Cordilleran ice sheet advanced southward into the Puget Sound ~17,500 yr ago, it dammed rivers flowing west from the Cascade Mountains (Porter and Swanson, 1998), filling the North Fork Stillaguamish River (NFSR) valley with 200 m of glacial sediment. Geologic mapping indicates that numerous landslides have occurred in this sediment (Dragovich et al., 2003), which is characterized by low-permeability glaciolacustrine clays overlain by sandy advance outwash, till, and gravelly recessional outwash (Keaton et al., 2014; Riemer et al., 2015). Similar stratigraphy is prevalent in the region and is well known to be landslide prone during and soon after high-intensity or long-duration precipitation (Chleborad, 2000; Coe et al., 2004).

Following ice retreat ~16.4 k.y. ago (Porter and Swanson, 1998; Beechie et al., 2001), the NFSR began incising rapidly into these mechanically weak glacial deposits, creating the modern valley relief and setting the stage for long-standing slope instability in the area.

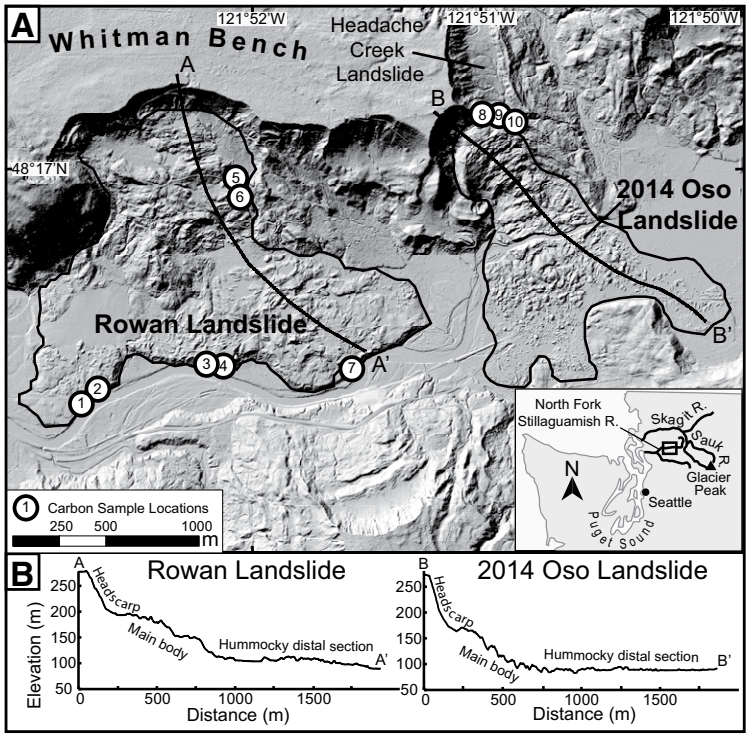

Figure 1. A: Lidar bare-earth imagery showing the Rowan landslide and the A.D. 2014 Oso landslide in the North Fork Stillaguamish River (R.) valley (Washington State, USA); ^{14}C samples are shown as numbered circles and the study area is shown as a black box in the inset map. B: Elevation profiles of the Rowan and 2014 Oso landslides.

GEOLOGY, February 2016; v. 44; no. 2; p. 111–114 | Data Repository item 2016029 | doi:10.1130/G37267.1 | Published online 22 December 2015

Incision rates slowed ~12.5 k.y. ago, when a lahar originating from Glacier Peak caused a significant area of the NFSR headwaters to be captured by the adjacent Sauk River (Beechie et al., 2001) (Fig. 1, inset map). Because large, unstable portions of relict glacial deposits remain in the valley, such as the Whitman Bench just north of the river (Fig. 1), the landscape is still rapidly evolving.

METHODS

In this study we combine a surface roughness analysis with radiocarbon dates, then use results from a numerical landscape evolution model to establish a roughness-age function for the study site. We first mapped all landslide deposits on 0.9 m resolution lidar bare-earth imagery, and measured head-scarp dimensions, deposit area, and H:L for each landslide to compare the style of past landslides (Table DR1 in the GSA Data Repository[1]). Remobilizations of older landslide deposits were mapped as separate events (for landslide delineation criteria, see the Data Repository).

We used radiocarbon dates of woody debris to obtain absolute ages for the Rowan landslide (Fig. 1, samples 1–6; this study) and Headache Creek landslide (Fig. 1, samples 8–10; Keaton et al., 2014). We also dated a terrace 4 m above the active river channel to assess the timing of river incision to near present-day base level. We use this terrace age as a maximum age constraint for landslides in the valley, because landslides overrun this terrace and are on the modern valley floor below (Fig. 1, sample 7).

Using these radiocarbon dates, we calibrate a surface roughness analysis to estimate the age of the undated landslides across the study area. Previous studies have used surface roughness as an age proxy for other depositional landforms, particularly alluvial fans (Matmon et al., 2006; Frankel and Dolan, 2007). Qualitative assessments of landslide morphology have been used to estimate landslide timing (Bell et al., 2012), and surface roughness specifically has been used for automated mapping of landslides (Booth et al., 2009) and assessment of activity within landslide complexes (McKean and Roering, 2004; Glenn et al., 2006). Here we calculate surface roughness for each landslide deposit using the average standard deviation of slope (SDS) within a 15 × 15 m roving window (Berti et al., 2013); this window size best captures the average wavelength of the of landslide hummocks in the study area (Fig. DR1).

In order to apply measures of SDS as a landslide age proxy, we assume that rough terrain features throughout the study area smooth through diffusion of sediment downslope at approximately the same rate due to the similar climate and lithology (Keaton et al., 2014). We also assume similar initial roughness for fresh landslide deposits; this is supported by the morphological similarity between most landslides in the study area. Although there is some variability in landslide area and H:L ratio, we see no correlation between these variables and standard deviation of slope (Fig. DR3).

The average SDS values for landslides of known age are plotted against four absolute age constraints on landsliding: the 2014 Oso landslide, the Rowan landslide, the Headache Creek landslide, and a maximum landslide age constrained by the age of the river terrace 4 m above the modern floodplain (which we assign to the landslide deposit with the lowest SDS value; Fig. 1, sample 7). We also employ a numerical landscape evolution model, which calculates SDS of the Oso landslide deposit at each time step for 12 k.y., to determine the regression that best represents the data (for model description, see the Data Repository).

RESULTS

Landslide Mapping

We remotely mapped 25 individual landslide deposits within a 6-km-long section of the NFSR valley, similar to what was mapped by Haugerud (2014). H:L analysis reveals several past landslides with considerable mobility, with 30% having H:L values of ≤0.20 (Table DR1). The largest landslide deposit in the valley, the Rowan landslide, covers nearly double the area of the 2014 Oso landslide (Fig. 1A) and exhibits an H:L ratio of 0.10, equal to that of the Oso landslide (Keaton et al., 2014; Iverson et al., 2015). The longitudinal morphology of the Rowan deposit also closely resembles that of the Oso landslide, with a steep main head scarp, similar extensional faulted blocks in the main body of the deposit, and a distal section where hummocks likely traveled on a more fluidized basal layer (Fig. 1B).

^{14}C Dating

Radiocarbon dates from six samples of wood entrained in the Rowan landslide deposit (Fig. 1, samples 1–6) yield ages between 694 and 300 calendar (cal) ^{14}C yr B.P., with an average age of 518 cal ^{14}C yr B.P. (Table DR2). Radiocarbon dates from the three samples at Headache Creek landslide (Fig. 1, samples 8–10 in) yield ages between 6278 and 5757cal ^{14}C yr B.P. (Table DR2). A tree trunk from within the fluvial terrace overrun by the Rowan landslide (Fig. 1, sample 7) dates to 11,978–11,406 cal ^{14}C yr B.P. (Table DR2), which agrees well with previous dating of NFSR terraces (Beechie et al., 2001).

Calibrated Surface Roughness Dating

When SDS is plotted against absolute age of the dated landslide deposits, these data show that landslide surface roughness decays with time at a decreasing rate (Fig. 2). Results from the numerical landscape evolution model suggest that the smoothing of landslide deposits over time is well fit by an exponential decay function (Fig. 2A; Fig. DR2). Fitting an exponential curve to the four observed roughness-age data points yields the following function: $t = 3519500 \times e^{-1.3976R}$, where t = estimated age (cal yr B.P.) and R = average SDS of landslide deposit (Fig. 2B). Using this function, we estimate the age of each landslide in the study area, and bin landslides into the following four age classes: A, >5000 yr B.P.; B, 2000–5000 yr B.P.; C, 500–2000 yr B.P.; D, <500 yr B.P. (Fig. 3).

DISCUSSION AND CONCLUSIONS

Results from this study show that SDS calculated from high-resolution elevation data can be a useful landslide dating tool. This technique enhances the value of a limited set of absolute dates by calibrating a surface roughness-age relationship that can be applied more broadly in development of regional landslide chronologies. Although we apply this approach exclusively to landslides in glacial sediment, bedrock landslides are likely to smooth more slowly, but at an equally predictable rate. If so, this method may be universally applicable in landslide-prone regions, so long as factors influencing initial landslide roughness are constant throughout the area being studied.

Using this approach, we show that the NFSR valley is a highly unstable postglacial landscape where the process of glacial sediment evacuation is ongoing, facilitated primarily though long-runout landslides. An average landslide frequency calculated using the total number of landslides in the study area and assuming no landslides are older than 12,000 yr yields a value of 1 event per 500 yr. However, the high number of young landslides here suggests a preservation bias caused by older landslide deposits being overrun by younger slope failures, or remobilization of older landslide deposits (Pánek et al., 2013). When only the past 2000 yr are considered, the average landslide frequency is substantially higher, 1 event per 140 yr.

Although the Oso and Rowan landslides have the lowest measured H:L ratios, many landslides in the valley with higher H:L ratios have been substantially eroded by the NFSR (Fig. 3B), such that the present-day length of deposits is not representative of the true runout length. Many of these landslides, particularly the multiple class A landslides in the southeast

[1]GSA Data Repository item 2016029, landslide mapping and delineation criteria, map of surface roughness within study area, landslide morphology data table, radiocarbon dating results, discussion of roughness-age calibration and description of landscape evolution model, and potential sources of error, is available online at www.geosociety.org/pubs/ft2016.htm, or on request from editing@geosociety.org or Documents Secretary, GSA, P.O. Box 9140, Boulder, CO 80301, USA.

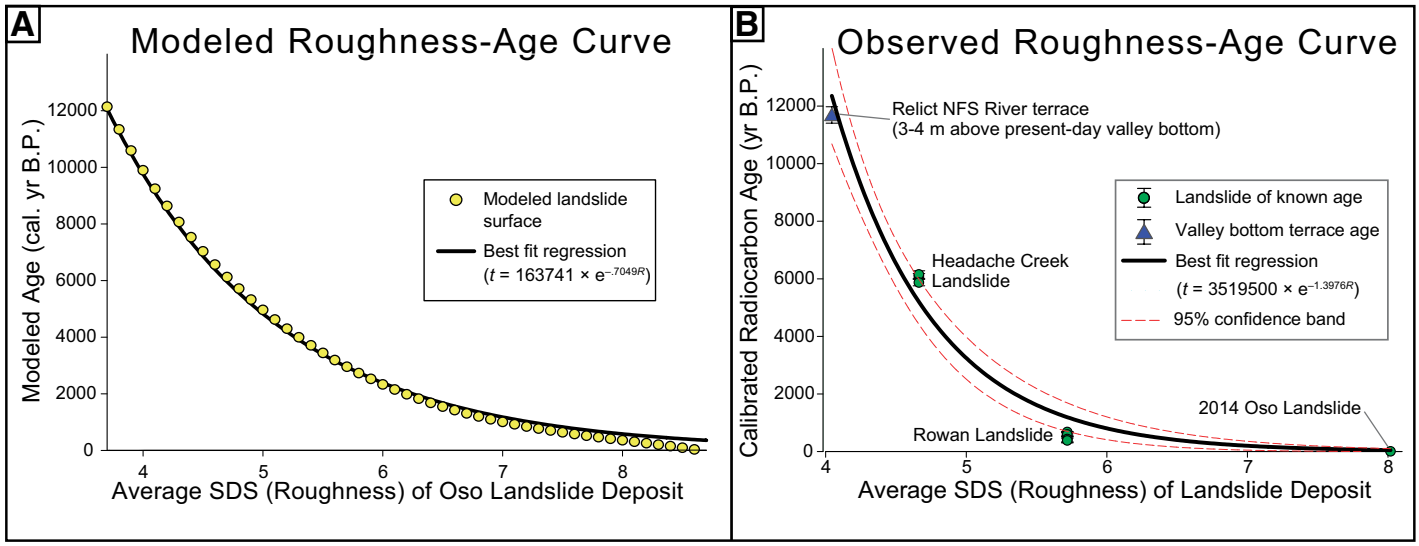

Figure 2. A: Exponential decay function fit to the linear diffusion model results, where the A.D. 2014 Oso landslide (Washington State, USA) elevation data are used as the initial condition at time *t* = 0. SDS—standard deviation of slope; cal. yr B.P.—calendar years before present. B: Exponential decay function fit to observed roughness-age data and used to estimate landslide age across the study area. Calibrated ^{14}C dates (present = 1950) are plotted against standard deviation of slope (roughness), with a maximum landslide age constrained by the age of a valley bottom terrace. NFS—North Fork Stillaguamish.

quadrant of the study area, have head scarp and deposit morphologies similar to those of the Oso and Rowan landslides, suggesting similar dynamics (Legros, 2002) and mobility (Fig. 3).

We suspect that mass-wasting events in the area are related to spatial patterns in NFSR erosion, and that landslides, in turn, impart a strong control on river location. Much of the NFSR floodplain was likely covered when the Rowan landslide occurred, pinning the river against the south side of the valley (Fig. 3B). A fluvial erosional contact evident in lidar images at the toe of an older landslide adjacent to the Rowan landslide suggests that the NFSR was once located on the north side of the valley, and was displaced ~600 m to the south by the Rowan landslide (Fig. 3B). Although the 2014 Oso landslide displaced the NFSR by ~150 m, it was less voluminous than the Rowan landslide (Iverson et al., 2015), and did not confine the river to the opposite side of the valley. This suggests that the lateral displacement of the river channel caused by a landslide is a product of both the mobility and volume of the landslide. When long-runout landslides of sufficient volume cover most of the valley floor, the river is forced to flow around the toe of the deposit, and fluvial erosion is concentrated where the channel is confined. We suspect that landslides from one side of the valley repeatedly set up slope failures to occur on the opposite side, over time creating an alternating pattern of landsliding (Safran et al., 2011).

The evidence for postglacial instability throughout the Holocene indicates that the mechanically weak glacial stratigraphy found in this valley, which is typical of ice-sheet advances around the world, presents an ongoing landslide hazard that will continue until the removal of this material from the valley. These slope failures in glacial sediment represent a distinctly different geomorphic system than that of postglacial bedrock landscapes, where landslide frequency decreases with time after ice retreat (Cruden and Hu, 1993). While bedrock landslides may contribute to overall landscape stability by reducing glacially oversteepened

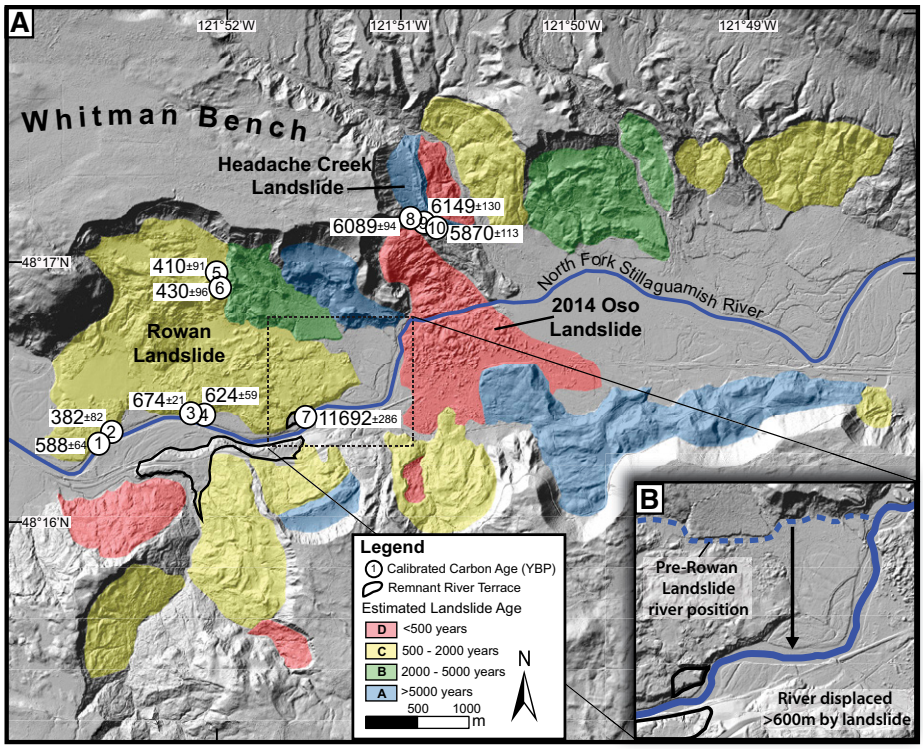

Figure 3. A: Lidar bare-earth imagery of the study area, showing all mapped landslides colored by estimated age. Landslides are binned into four age classes (7 class A, 3 class B, 10 class C, and 5 class D; see text) based on estimated age from the surface roughness-age regression. Predicted age classes agree well with crosscutting relationships between landslides. cal yr B.P.—years before present (present = 1950). B: Blow-up map showing inferred river position (dashed line) prior to the Rowan landslide (Washington State, USA) ca. 500 ^{14}C yr B.P., based on erosional contact on an older landslide deposit. The current river position (solid line) suggests that the active channel was displaced at least 600 m when the Rowan landslide occurred.

slopes, landslides in glacial sediment often do not require steep slopes to fail (Geertsema et al., 2006), and perpetuate further landsliding by debuttressing adjacent material. Therefore, even in the absence of rapid uplift or incision, the process of evacuating potentially unstable glacial sediment may result in persistent instability for tens of thousands of years after ice retreat, placing this process at the upper limit of estimations of paraglacial landscape relaxation time scales (Ballantyne, 2002). The longevity of landslide hazard in such regions accentuates the need for accurate and robust landslide chronologies. Our analysis shows that remote sensing data can be used to quantitatively estimate landslide age, and thereby assess landslide risk, when surface roughness is calibrated with even a limited set of absolute dates.

ACKNOWLEDGMENTS

We acknowledge the National Science Foundation (grant EAR-1331412), the Geological Society of America (graduate student grant to LaHusen), and the University of Washington Quaternary Research Center for support of this research. We thank the Washington Department of Natural Resources for site access and Stephen Slaughter and Camille Collett for assistance in the field. This manuscript benefited greatly from discussions with Amit Mushkin and thoughtful reviews by two anonymous reviewers and the editor.

REFERENCES CITED

Ballantyne, C.K., 2002, Paraglacial geomorphology: Quaternary Science Reviews, v. 21, p. 1935–2017, doi:10.1016/S0277-3791(02)00005-7.

Beechie, T.J., Collins, B.D., and Pess, G.R., 2001, Holocene and recent geomorphic processes, land use, and salmonid habitat in two north Puget Sound river basins, *in* Dorava, J.M., et al., eds., Geomorphic processes and riverine habitat: American Geophysical Union Water Science and Application, v. 4, p. 37–54, doi:10.1029/WS004p0037.

Bell, R., and Glade, T., 2004, Quantitative risk analysis for landslides—Examples from Bíldudalur, NW Iceland: Natural Hazards and Earth System Sciences, v. 4, p. 117–131, doi:10.5194/nhess-4-117-2004.

Bell, R., Petschko, H., Roehrs, M., and Dix, A., 2012, Assessment of landslide age, landslide persistence and human impact using airborne laser scanning digital terrain models: Geografiska Annaler, ser. A, v. 94, p. 135–156, doi:10.1111/j.1468-0459.2012.00454.x.

Berti, M., Corsini, A., and Daehne, A., 2013, Comparative analysis of surface roughness algorithms for the identification of active landslides: Geomorphology, v. 182, p. 1–18, doi:10.1016/j.geomorph.2012.10.022.

Booth, A.M., Roering, J.J., and Perron, J.T., 2009, Automated landslide mapping using spectral analysis and high-resolution topographic data: Puget Sound lowlands, Washington, and Portland Hills, Oregon: Geomorphology, v. 109, p. 132–147, doi:10.1016/j.geomorph.2009.02.027.

Chleborad, A.F., 2000, Preliminary method for anticipating the occurrence of precipitation-induced landslides in Seattle, Washington: U.S. Geological Survey Open-File Report 2000-469, 29 p., http://pubs.usgs.gov/of/2000/0469/report.pdf.

Coe, J.A., Michael, J.A., Crovelli, R.A., Savage, W.Z., Laprade, W.T., and Nashem, W.D., 2004, Probabilistic assessment of precipitation-triggered landslides using historical records of landslide occurrence, Seattle, Washington: Environmental & Engineering Geoscience, v. 10, p. 103–122, doi:10.2113/10.2.103.

Cruden, D.M., and Hu, X.Q., 1993, Exhaustion and steady state models for predicting landslide hazards in the Canadian Rocky Mountains: Geomorphology, v. 8, p. 279–285, doi:10.1016/0169-555X(93)90024-V.

Dragovich, J., Stanton, B., Lingley, W., Griesel, G., and Polenz, M., 2003, Geologic map of the Mount Higgins 7.5-minute quadrangle, Skagit and Snohomish Counties, Washington: Washington Division of Geology and Earth Resources Open-File Report 2003-12, scale 1:24,000.

Frankel, K.L., and Dolan, J.F., 2007, Characterizing arid region alluvial fan surface roughness with airborne laser swath mapping digital topographic data: Journal of Geophysical Research, v. 112, F02025, doi:10.1029/2006JF000644.

Geertsema, M., Clague, J.J., Schwab, J.W., and Evans, S.G., 2006, An overview of recent large catastrophic landslides in northern British Columbia, Canada: Engineering Geology, v. 83, p. 120–143, doi:10.1016/j.enggeo.2005.06.028.

Glenn, N.F., Streutker, D.R., Chadwick, D.J., Thackray, G.D., and Dorsch, S.J., 2006, Analysis of LiDAR-derived topographic information for characterizing and differentiating landslide morphology and activity: Geomorphology, v. 73, p. 131–148, doi:10.1016/j.geomorph.2005.07.006.

Haugerud, R.A., 2014, Preliminary interpretation of pre-2014 landslide deposits in the vicinity of Oso, Washington: U.S. Geological Survey Open-File Report 2014-1065, 4 p., doi:10.3133/ofr20141065.

Iverson, R.M., et al., 2015, Landslide mobility and hazards: Implications of the 2014 Oso disaster: Earth and Planetary Science Letters, v. 412, p. 197–208, doi:10.1016/j.epsl.2014.12.020.

Keaton, J.K., Wartman, J., Anderson, S., Benoît, J., deLaChapelle, J., Gilbert, R., and Montgomery, D.R., 2014, The 22 March 2014 Oso Landslide, Snohomish County, Washington: Geotechnical Extreme Events Reconnaissance Association Report GEER-036, 186 p., http://snohomishcountywa.gov/DocumentCenter/View/18180.

Lang, A., Moya, J., Corominas, J., Schrott, L., and Dikau, R., 1999, Classic and new dating methods for assessing the temporal occurrence of mass movements: Geomorphology, v. 30, p. 33–52, doi:10.1016/S0169-555X(99)00043-4.

Legros, F., 2002, The mobility of long-runout landslides: Engineering Geology, v. 63, p. 301–331, doi:10.1016/S0013-7952(01)00090-4.

Matmon, A., Nichols, K., and Finkel, R., 2006, Isotopic insights into smoothening of abandoned fan surfaces, southern California: Quaternary Research, v. 66, p. 109–118, doi:10.1016/j.yqres.2006.02.010.

McKean, J., and Roering, J., 2004, Objective landslide detection and surface morphology mapping using high-resolution airborne laser altimetry: Geomorphology, v. 57, p. 331–351, doi:10.1016/S0169-555X(03)00164-8.

Morgan, G.C., Rawlings, G.E., and Sobkowicz, J.C., 1992, Evaluating total risk to communities from large debris flows, *in* Proceedings, Geotechnique and Natural Hazards Symposium, Vancouver, BC, Vancouver Geotechnical Society and Canadian Geotechnical Society, May 6–9, 1992: Vancouver, Canada, Bitech Publishers, p. 6–9.

Pánek, T., 2015, Recent progress in landslide dating: Progress in Physical Geography, v. 39, p. 168–198, doi:10.1177/0309133314550671.

Pánek, T., Smolková, V., Hradecký, J., Baroň, I., and Šilhán, K., 2013, Holocene reactivations of catastrophic complex flow-like landslides in the Flysch Carpathians (Czech Republic/Slovakia): Quaternary Research, v. 80, p. 33–46, doi:10.1016/j.yqres.2013.03.009.

Porter, S.C., and Swanson, T.W., 1998, Radiocarbon age constraints on rates of advance and retreat of the Puget lobe of the Cordilleran ice sheet during the last glaciation: Quaternary Research, v. 50, p. 205–213, doi:10.1006/qres.1998.2004.

Riemer, M.F., Collins, B., Badger, T.C., Toth, C., and Yu, Y.C., 2015, Geotechnical soil characterization of intact Quaternary deposits forming the March 22, 2014 SR-530 (Oso) landslide, Snohomish County, Washington: U.S. Geological Survey Open-File Report 2015-1089, 17 p., doi:10.3133/ofr20151089

Roering, J.J., Mackey, B.H., Marshall, J.A., Sweeney, K.E., Deligne, N.I., Booth, A.M., Handwerger, A.L., and Cerovski-Darriau, C., 2013, 'You are here': Connecting the dots with airborne lidar for geomorphic fieldwork: Geomorphology, v. 200, p. 172–183, doi:10.1016/j.geomorph.2013.04.009.

Safran, E.B., Anderson, S.W., Mills-Novoa, M., House, P.K., and Ely, L., 2011, Controls on large landslide distribution and implications for the geomorphic evolution of the southern interior Columbia River basin: Geological Society of America Bulletin, v. 123, p. 1851–1862, doi:10.1130/B30061.1.

Sterlacchini, S., Frigerio, S., Giacomelli, P., and Brambilla, M., 2007, Landslide risk analysis: A multi-disciplinary methodological approach: Natural Hazards and Earth System Sciences, v. 7, p. 657–675, doi:10.5194/nhess-7-657-2007.

Manuscript received 16 August 2015
Revised manuscript received 26 November 2015
Manuscript accepted 2 December 2015

Printed in USA